Published in final edited form as:
Neuroimage. 2013 January 1; 64: 671–684. doi:10.1016/j.neuroimage.2012.09.004.

Development of Brain Structural Connectivity between Ages 12 and 30: A 4-Tesla Diffusion Imaging Study in 439 Adolescents and Adults

Emily L. Dennis[1], **Neda Jahanshad**[1], **Katie L. McMahon**[2], **Greig I. de Zubicaray**[3], **Nicholas G. Martin**[4], **Ian B. Hickie**[5], **Arthur W. Toga**[6], **Margaret J. Wright**[3,4], and **Paul M. Thompson**[1]

[1]Imaging Genetics Center, Laboratory of Neuro Imaging, UCLA School of Medicine, Los Angeles, CA, USA

[2]Center for Advanced Imaging, Univ. of Queensland, Brisbane, Australia

[3]School of Psychology, University of Queensland, Brisbane, Australia

[4]Queensland Institute of Medical Research, Brisbane, Australia

[5]Brain and Mind Research Institute, University of Sydney, Australia

[6]Laboratory of Neuro Imaging, UCLA School of Medicine, Los Angeles, CA, USA

Abstract

Understanding how the brain matures in healthy individuals is critical for evaluating deviations from normal development in psychiatric and neurodevelopmental disorders. The brain's anatomical networks are profoundly re-modeled between childhood and adulthood, and diffusion tractography offers unprecedented power to reconstruct these networks and neural pathways *in vivo*. Here we tracked changes in structural connectivity and network efficiency in 439 right-handed individuals aged 12 to 30 (211 female/126 male adults, mean age=23.6, SD=2.19; 31 female/24 male 12 year olds, mean age=12.3, SD=0.18; and 25 female/22 male 16 year olds, mean age=16.2, SD=0.37). All participants were scanned with high angular resolution diffusion imaging (HARDI) at 4 Tesla. After we performed whole brain tractography, 70 cortical gyral-based regions of interest were extracted from each participant's co-registered anatomical scans. The degree of fiber connections between all pairs of cortical regions, or nodes, were found to create symmetric fiber density matrices, reflecting the structural brain network. From those 70×70 matrices we computed graph theory metrics characterizing structural connectivity. Several key global and nodal metrics changed across development, showing increased network integration, with some connections pruned and others strengthened. The increases and decreases in fiber density, however, were not distributed proportionally across the brain. The frontal cortex had a disproportionate number of decreases in fiber density while the temporal cortex had a disproportionate number of increases in fiber density. This large-scale analysis of the developing

Please address correspondence to: Paul Thompson, PhD, Professor of Neurology, Laboratory of Neuro Imaging, Department of Neurology, UCLA School of Medicine, 635 Charles Young Drive South, Suite 225, Los Angeles, CA 90095-7334, 310-206-2101, thompson@loni.ucla.edu.

Author Disclosure Statement: The authors have no competing financial interests.

structural connectome offers a foundation to develop statistical criteria for aberrant brain connectivity as the human brain matures.

Keywords

HARDI; structural connectivity; graph theory; development

1. Introduction

The human brain changes profoundly, both functionally and structurally, between childhood and adulthood (Dosenbach et al., 2010; Gogtay et al., 2004; Lenroot et al., 2007; Sowell et al., 2003; Shaw et al., 2008). Following the massive growth in the number of synapses after birth, anatomical studies show a decline in synaptic density, as short-range connections are pruned in favor of long-range ones (Huttenlocher, 1979; Huttenlocher, 1990). Studies of structural connectivity using diffusion imaging show that the fractional anisotropy of water along white matter tracts – an index of myelination and axonal coherence – increases in childhood, plateaus in adulthood, and declines in old age (Kochunov et al., 2010). Studies of functional connectivity have employed resting-state fMRI data to estimate the "developmental ages" or relative maturity of participants, finding that chronological age accounts for over half of the variance in functional brain connectivity in developmental samples (Dosenbach et al., 2010). Defining the developmental trajectory for various measures of brain structure and function is critical for understanding general principles of neural network development. Determining the normal developmental trajectory will also help to identify deviations in structural circuitry implicated in neuropsychiatric disorders such as autism or schizophrenia (Scott-Van Zeeland et al., 2010).

Graph theory is a branch of mathematics developed to describe and analyze networks, offering a variety of metrics that have become popular for characterizing networks in the brain. By modeling the brain as a collection of nodes (hubs) and edges (connections between them), graph theory quantifies network topology through a number of standard parameters (Sporns et al., 2004). One of these is path length, a measure of the distance, in edges, between one brain region (node) and another (Rubinov & Sporns, 2010). Global efficiency is the inverse of path length – networks with shorter average path lengths are generally more efficient in transferring information. These metrics are genetically influenced (Dennis et al., 2011) and their properties are known to depend on specific genetic variants in normal adults and cognitively impaired adults (Brown et al., 2011; Dennis et al., 2012a).

To date, a few studies have begun to assess how graph theory metrics of structural connectivity change during development. Gong et al. (2009) examined anatomical connectivity in 95 subjects aged 19–85. Hagmann et al. (2010), tracked white matter maturation in 30 subjects between 18 months and 18 years of age. We were particularly interested in the developmental period from early adolescence to early adulthood, when the brain fully matures. The pioneering study by Hagmann and colleagues was limited by small sample size (30 subjects), so we set out to chart the developmental trajectory of network metrics in a much larger cross-sectional sample (439 subjects).

To map structural brain connectivity between childhood and adulthood, we scanned 439 subjects between ages 12 and 30, with high-field (4-Tesla) high angular resolution diffusion imaging (HARDI). We computed standard graph theory metrics from 70×70 connectivity matrices of fiber density. These connection matrices were probed for linear and non-linear relationships with age. We hypothesized that we would find evidence of decreased path length with age, reflecting a developmental process of pruning short-range connections and

strengthening long-range connections (Casey et al., 2000; Hagmann et al., 2010; Thomason et al., 2010).

2. Material and methods

2.1 Participants

Participants were recruited as part of a 5-year research project examining healthy Australian twins with structural MRI and diffusion weighted imaging, with a projected sample size of approximately 1150 at completion (de Zubicaray et al., 2008). Our analysis included 439 right-handed subjects (adult sample: 211 females/126 males, mean age=23.6, SD=2.19; 12 year old sample: 31 females/24 males, mean age=12.3, SD=0.18; 16 year old sample: 25 females/22 males, mean age=16.2, SD=0.37). This population included 146 monozygotic (MZ) twins, 259 dizygotic (DZ) twins, and 34 non-twin siblings, from 275 families. 337 were adults, 55 were adolescents, and 47 were children, shown in Table 1. Since our current focus is on description of network growth trajectories, the present analyses make no use of twin relatedness to estimate genetic and environmental components.

The population was racially homogeneous: 100% of subjects were Caucasian. Subjects were screened to exclude those with a history of significant head injury, neurological or psychiatric illness, substance abuse or dependence, or had a first-degree relative with a psychiatric disorder. All participants were right-handed, as assessed by 12 items on the Annett's Handedness Questionnaire (Annett et al., 1970). The adult cohort and the 16 year old cohort both completed the Multidimensional Aptitude Battery II (MAB-II) IQ test (Jackson, 1998). Most participants who completed the MAB-II did so at age 16 (92%); the others completed the MAB-II at a later session, some at the scan session (4% were between 17–20 years, 3% were between 20–23 years, 1% were between 25–29 years). The 12-year-old cohort did not complete the MAB IQ scale. Study participants gave informed consent; institutional ethics committees at the Queensland Institute of Medical Research, the University of Queensland, the Wesley Hospital, and at UCLA approved the study. The adult subjects in this sample partially overlap with a sample examined in prior studies (Braskie et al., 2011; Braskie et al., 2012), which revealed single-gene effects on measures of brain integrity and connectivity, but did not assess children.

2.2 Scan Acquisition

Whole-brain anatomical and high angular resolution diffusion images (HARDI) were collected with a 4T Bruker Medspec MRI scanner. T1-weighted anatomical images were acquired with an inversion recovery rapid gradient echo sequence. Acquisition parameters were: TI/TR/TE = 700/1500/3.35ms; flip angle = 8 degrees; slice thickness = 0.9mm, with a 256×256 acquisition matrix. HARDI was also acquired using single-shot echo planar imaging with a twice-refocused spin echo sequence to reduce eddy-current induced distortions. Imaging parameters were: 23cm FOV, TR/TE 6090/91.7ms, with a 128×128 acquisition matrix. Each 3D volume consisted of 55 2-mm thick axial slices with no gap and 1.79×.1.79 mm^2 in-plane resolution. 105 images were acquired per subject: 11 with no diffusion sensitization (i.e., T2-weighted b_0 images) and 94 diffusion-weighted (DW) images ($b = 1159$ s/mm^2) with gradient directions evenly distributed on a hemisphere in the q-space. Some subjects' HARDI scans were acquired with a 77-gradient protocol ($b = 1177$ s/mm^2), as the 105-gradient protocol was too long for some adolescents to sit through. We have previously undertaken several detailed studies (Zhan et al., 2009; Zhan et al., 2012a,b) to determine how angular and spatial resolution affect brain connectivity maps, and the results and stability at high numbers of diffusion gradients are reported in those papers. The number of gradients affects the accuracy of reconstruction of the diffusion profile, but by the time 50–60 gradients are reached, the primary measures of diffusion, including the principal

eigenvector, have converged (Zhan et al., 2008, Zhan et al., 2009b,c). The connectivity matrix has been found to depend more on the voxel size than the number of gradients, and the voxel size was kept the same in the adolescents. Scan time for the 105-gradient HARDI scan was 14.2 min. Scan time for the 77-gradient HARDI scan was 10.8 min.

2.3 Cortical Extraction and HARDI Tractography

Connectivity analysis was performed exactly as in Jahanshad et al. (2011). Briefly, non-brain regions were automatically removed from each T1-weighted MRI scan using ROBEX (JE Iglesias, TMI 2011), and from a T2-weighted image from the DWI set, using the FSL tool "BET" (FMRIB Software Library, http://fsl.fmrib.ox.ac.uk/fsl/). Intracranial volume estimates were obtained from the full brain mask, and included cerebral, cerebellar, and brain stem regions. All T1-weighted images were linearly aligned using FSL (with 9 DOF) to a common space (Holmes et al., 1998) with $1mm$ isotropic voxels and a 220×220×220 voxel matrix. Raw diffusion-weighted images were corrected for eddy current distortions using the FSL tool, "eddy_correct". For each subject, the 11 eddy-corrected images with no diffusion sensitization were averaged, linearly aligned and resampled to a downsampled version of their corresponding T1 image (110×110×110, 2×2×2mm). Averaged b_0 maps were elastically registered to the structural scan using a mutual information cost function (Leow et al., 2005) to compensate for EPI-induced susceptibility artifacts.

35 cortical labels per hemisphere, as listed in the Desikan-Killiany atlas (Desikan et al., 2006), were automatically extracted from all aligned T1-weighted structural MRI scans using FreeSurfer (http://surfer.nmr.mgh.harvard.edu/). As a linear registration is performed by the software, the resulting T1-weighted images and cortical models were aligned to the original T1-weighted input image space and down-sampled using nearest neighbor interpolation (to avoid intermixing of labels) to the space of the DWIs. To ensure tracts would intersect cortical labeled boundaries, labels were dilated with an isotropic box kernel of width 5 voxels.

The transformation matrix from the linear alignment of the mean b_0 image to the T1-weighted volume was applied to each of the 94 gradient directions to properly reorient the orientation distribution functions (ODFs). At each HARDI voxel, ODFs were computed using the normalized and dimensionless ODF estimator, derived for q-ball imaging (QBI) in (Aganj et al., 2010). We performed HARDI tractography on the linearly aligned sets of DWI volumes using these ODFs. Tractography was performed using the Hough transform method as described in (Aganj et al., 2011).

Elastic deformations obtained from the EPI distortion correction, mapping the average b_0 image to the T1-weighted image, were then applied to the tracts' 3D coordinates for accurate alignment of the anatomy. Each subject's dataset contained 5,000–10,000 useable fibers (3D curves). Fibers were filtered to eliminate those that may have arbitrarily been drawn on the brain-boundary due to noise and high FA. All duplicate fibers were removed.

For each subject, a full 70×70 connectivity matrix was created. Each element described the proportion of the total number of fibers connecting each of the labels; diagonal elements of the matrix describe the total number of fibers passing through a certain cortical region of interest. These values were calculated as a proportion - they were normalized to the total number of fibers traced for each person in the study - so that results were not skewed by raw fiber count.

2.4 Graph Theory Analyses

On the 70×70 matrices generated above, we used the Brain Connectivity Toolbox (Rubinov & Sporns, 2010; https://sites.google.com/a/brain-connectivity-toolbox.net/bct/Home) to

compute seven standard measures of global brain connectivity - characteristic path length (CPL), mean clustering coefficient (MCC), global efficiency (EGLOB), small-worldness (SW), and modularity (MOD), as well as normalized path length (lambda) and normalized clustering coefficient (gamma). CPL measures the average path length in a network, where the path length is defined as the minimum number of edges that must be traversed to get from one node to another (note this depends on the number of nodes traversed, and does not depend on the physical length of axons or how they are organized spatially in the brain). MCC is a measure of how many neighbors of a given node are also connected to each other, in proportion to the maximum number of connections in the network. EGLOB is inversely related to CPL: networks with a small average CPL are generally more efficient than those with large average CPL. SW represents the balance between network differentiation and network integration, calculated as a ratio of local clustering and characteristic path length of a node relative to the same ratio in a randomized network. We created 15 simulated random networks. The ratio of clustering in our network to the average clustering in a simulated random network – with the same number of nodes and connections – is gamma, while the ratio of characteristic path length in our network to the average path length in a simulated random network is lambda. MOD is the degree to which a system may be subdivided into smaller networks (Bullmore & Bassett, 2010). We also calculated 4 standard nodal measures of connectivity – regional efficiency (EREG), “betweenness centrality” (BC), degree, and clustering coefficient (CC). EREG is the global efficiency computed for each node and is related to the clustering coefficient (Latora & Marchiori, 2001). BC is the fraction of all of the shortest paths in a network that contain a given node with higher numbers indicating participation in a large number of shortest paths (Kintali, 2008). Degree is the number of links (edges) connected to a node (Sporns, 2002). Equations to calculate these measures may be found in Rubinov and Sporns (2010).

One possible step in graph theory analyses is selecting a sparsity, which is related to thresholding the network (removing nodes and edges based on their weightings). The sparsity is the fraction of connections retained from the full network: setting a sparsity level of 0.2 means that only the top 20% of connections are retained for calculations. Selecting a single sparsity level may arbitrarily affect the network measures, so we computed measures at multiple sparsities, and integrated the measures across that range to generate more stable scores. As noted in Dennis et al. (2012b), the sparsity (threshold) determines which nodes remain in a network and is typically defined with the goal of eliminating noisy or unreliable connections. To minimize any effects of arbitrary thresholding, we calculated our network measures over a range of thresholds (Achard & Bullmore, 2007; Bassett et al., 2008; He et al., 2008; Khundrakpam et al., 2012;) and integrated over that range. We have shown this can improve their robustness and test-retest reliability (Dennis et al., 2012c). We selected the range 0.2–0.3 to calculate and integrate these measures, as that range is biologically plausible (Sporns, 2011) and more stable (Dennis et al., 2012a). We calculated these measures for the whole brain over a range of sparsities (0.2–0.3, in 0.01 increments), and calculated the area under the curve of those 11 data points to generate an integrated score for each measure. We also computed network measures for the left and right hemispheres independently.

2.5 Age Regression

Age-related effects on graph theory metrics of structural brain connectivity were estimated using a general linear model including mixed effects, as well as a simpler linear mixed effects model, as follows:

$$\text{Graph theory metrics} \sim A + \beta_{age}\text{Age} + \beta_{sex}\text{Sex} + \beta_{ICV}\text{ICV} + \beta_{age^2}\text{Age}^2 + \alpha + \varepsilon \quad \text{(Eq. 1)}$$

$$\text{Graph theory metrics} \sim A + \beta_{\text{age}}\text{Age} + \beta_{\text{sex}}\text{Sex} + \beta_{\text{ICV}}\text{ICV} + \alpha + \varepsilon \quad \text{(Eq. 2)}$$

Here, "graph theory metrics" could be any of CPL, MCC, EGLOB, SW, MOD, lambda, or gamma. A is the constant graph theory metric term, the βs are the covariate regression coefficients, and α is a coefficient that accounts for random effects. Random effects were used to account for familial relatedness. Both *age* and age^2 were included as variables to model both linear and non-linear age effects. We modeled these variables (*age*, sex, ICV, age^2) as fixed effects. We initially included an interaction term, *age**sex, as well, but it was not kept in the model as it did not fit. ICV denotes intracranial volume, in mm^3. We additionally tested the raw 70×70 fiber density matrices on an element-by-element basis to test for any effects of *age* and age^2, using the same models as above.

3. Results

3.1 Whole Brain Analyses

The model that included *age* and age^2 together, with sex and ICV as additional covariates (as shown in Eq. 1), revealed significant linear trends of decreasing CPL, lambda (normalized path length), gamma (normalized clustering coefficient), SW, and MOD with age. Most of these also had a significant age^2 term in the *opposite* direction, indicating an age effect that leveled off. This slowing down of the age effect would be expected, in early adulthood. Scatterplots of these results, and those for the left and right hemispheres treated separately, are shown in Figure 1. Studies of sex differences in graph theoretical measures of structural brain connectivity are few (Gong et al., 2011; Yan et al., 2011). From these few studies we expected females to have higher global efficiency and higher regional efficiency in temporal nodes. We also expected males to have higher regional efficiency in frontal nodes. We found significant sex effects for SW and gamma. For both, females tended to have greater values than males. The model described by Eq. 2, modeling *age*, sex, and ICV yielded significant age effects for CPL, gamma, and SW, with all of them decreasing with age, as hypothesized. The beta coefficients and corresponding *p*-values for these whole brain analyses are shown in Table 2. We also found a borderline significant sex effect (it did not survive multiple comparison correction for the number of whole brain global measures tested within this model, FDR correction) for SW for this model. Results were all corrected for multiple comparisons using the false discovery rate method (FDR; Benjamini & Hochberg, 1995). Linear best-fit lines are charted in Figure 1, with their regression coefficients, or estimated slopes. These linear trend lines and *b* values come from the regression model including sex and ICV as covariates, not simply age and the BCT measure of interest. The regression coefficients (*b* values) for *age* and age^2 are often of opposite sign, meaning that as we adjust for one covariate, the other tends to fit in the opposite direction. This indicates a plateau in adulthood, in line with intuition and empirical data on developmental trajectories for other anatomical measures (Thompson et al., 2005).

3.2 Left Hemisphere Analyses

When restricted to the intra-hemispheric connections within the left hemisphere (meaning those that began *and* terminated at left hemisphere nodes), the simpler linear model with only *age* described by Eq. 2 yielded significant results for MCC, EGLOB, and MOD, as well as borderline significant results for lambda and gamma. FDR correction for multiple comparisons was applied across the left and right hemisphere analyses together, within model ($q = 0.05$). The beta coefficients and corresponding *p*-values for the whole-brain analyses are presented in Table 3 and Figure 1. There were no significant sex effects for the left hemisphere analyses.

3.3 Right Hemisphere Analyses

The model with *age* and age^2 together (Eq. 1), when restricted to only intra-hemispheric connections within the right hemisphere, yielded borderline significant results for MCC, gamma, SW, and MOD ($p < 0.05$) but not FDR correction. The simpler model with only *age* described by Eq. 2 yielded significant results for MCC, gamma, EGLOB, SW, and MOD. The beta coefficients and corresponding *p*-values for whole brain analyses are shown in Table 4 and Figure 1. Results are FDR corrected across left and right hemisphere analyses within model for multiple comparisons ($q = 0.05$). There were sex effects for SW in the right hemisphere, but they only survived FDR for the model described by Eq. 2.

3.4 Nodal Analyses

Analyses of nodal measures of connectivity (regional efficiency - EREG, degree, clustering coefficient - CC, and betweenness centrality - BC) yielded a number of significant results for the model described by Eq. 1, which are shown in Table 5. When *age* was assessed alone (Eq. 2), age showed effects on several nodal measures (Table 6). Results are FDR corrected for multiple comparisons within model across all nodes and across all four metrics tested ($q = 0.05$). Details of how the significant changes break down by lobe can be found in Table 7. Figure 2 summarizes the developmental results, showing the differences in paths between groups and the differences in degree at certain nodes. Additionally, Supplementary Video 1 and Supplementary Video 2 online and Figure 3 display the increases and decreases, respectively, in degree and fiber density across ages 12–30. While we lack scan data for some parts of the age range, we used the regression coefficients from our analysis to estimate network metrics at each year.

3.5 70×70 Fiber Density Matrices

As we found significant results at the hierarchical levels, we also examined the original 70×70 fiber density matrices, from which these metrics were calculated, for age effects to focus on specific connections. When modeled together (Eq. 1), we found 112 connections with a significant association with *age* and 50 connections with a significant association with age^2, out of 1280 connections tested. We ran our analyses in two different ways – the first analysis examined connections existing in at least 95% of subjects, designed to reveal connections that exist in all age groups but change in fiber density. The second kind of analysis examined connections existing in at least 5% of subjects, designed to reveal connections that are gained or lost with age. Out of 2485 possible connections (70×70, symmetrical), we tested only those where at least 5% of subjects had a connection, resulting in 1280 connections tested. When effects of *age* were modeled alone (Eq. 2), we found 483 connections with a significant association with age, as shown in Figure 4. Results are FDR-corrected across all tested connections ($q = 0.05$). When *age* was modeled alone, and analyses were restricted to only connections present in at least 95% of subjects, there were 309 connections tested, 213 of which survived FDR, also shown in Figure 4. Table 8 shows the top 10 increases and top 10 decreases – i.e. those with the most significant age association (based on lowest p-value) when age was modeled alone and analyses were restricted to connections present in at least 95% of subjects. The left hemisphere is over-represented in these most significant results, perhaps due to the greater effect sizes in the left hemisphere than in the right. There were more connections that decreased in proportional fiber density than increased. The overall number of connections did not change with age; changes were seen in the proportional fiber density of specific connections. Fiber decreases were disproportionally seen in the frontal cortex, while the temporal cortex had disproportionally more fiber density increases.

These analyses were all performed on matrices than had been normalized by the number of fibers tracked, meaning that the results depict changes in proportional fiber density rather

than absolute fiber density. However, when analyses were run on the absolute fiber density data, the results were generally unchanged. Compared to the 213 connections found to have a significant age effect on the proportional fiber density data, the absolute fiber density age analysis revealed 220 significant connections. 203 of the 220 significant connections from the absolute fiber density analysis were the same ones that showed significance in the proportional fiber density analysis. 17 new connections were found in the absolute analysis and 10 connections that had been significant in the proportional fiber density analysis were no longer significant in the absolute fiber density analysis. Importantly, however, all significant results were in the same direction, so decreases in proportional fiber density are in fact true decreases in absolute fiber density, and do not simply imply that some connections are increasing to a lesser degree than the average. Figure 5 shows the developmental trajectory for 70×70 connections and degree, with an average network shown for each group. Supplementary Video 1 and Supplementary Video 2 online, and Figure 3 display these changes as well.

3.6 Cross-Hemisphere Connections

Of the 213 connections that survived FDR correction above, 9 were interhemispheric connections. We decided to further examine cross-hemisphere connections by restricting our 70×70 matrices to just assess interhemispheric connections. Of the 20 connections tested, 7 connections showed an age effect – those between the left isthmus of the cingulate and the right posterior cingulate, the left posterior cingulate and right paracentral gyrus, the left and right posterior cingulate, the left posterior cingulate and right precuneus, the left posterior cingulate and right superior frontal gyrus, the left precuneus and the right posterior cingulate, and the left superior frontal gyrus and right precuneus. All of these increased in fiber density with age (Figure 6).

3.7 Sex Differences

In addition to the sex differences found above, there were also a few differences in nodal measures of EREG and degree. While few, these results do fit with previous ones from Gong et al. (2009). These are shown in Table 8 and Figure 7. Results are FDR corrected (q = 0.05) with respect to the total number of nodes and measures tested.

4. Discussion

The current study sought to characterize the developmental trajectory of graph theory metrics of structural connectivity from early adolescence to early adulthood. Although our study was cross-sectional, its sample size was much larger than most prior studies of the developing structural connectome, offering greater power to detect age effects. The brain continues to mature into the twenties (Gogtay et al., 2004) and myelination and network remodeling continue throughout life (Bartzokis, 2004). Between ages 12 and 30, we found a number of linear and nonlinear age effects across the whole brain, for left and right hemispheres, and for specific nodes. These age effects were also seen in the connectivity matrices that served as the basis to compute the graph theory metrics, with significant age effects on fiber density. We also found significant sex differences in a few nodal measures.

For the whole-brain graph theory measures, we found significant effects of decreasing path length, clustering, small-worldness, and modularity with age, and all of these plateaued in early adulthood. Changes in “small-worldness” reflect a network property that itself depends on changes in either normalized clustering coefficient (gamma), normalized path length (lambda), or the ratio between those two. In our results it appears that it was the ratio between these two that changed, as gamma decreased at a faster rate than did lambda. These results are mostly in line with those of Hagmann et al. (2010), who also reported decreased

clustering and small-worldness in a much smaller sample of 30 subjects. The global results of decreasing path length, clustering, and modularity suggest that structural network integration increases during the teenage years. All subjects, regardless of age, showed a small-world topology in their brain networks. Adolescence is marked by parallel decreases in gray matter density, due in part to synaptic pruning (Gogtay et al., 2004), and increases in intracortical myelination through young adulthood (Giedd et al., 1999). As some short-range connections are pruned and other long-range ones are strengthened (Casey et al., 2000; Hagmann et al., 2010; Thomason et al., 2010), we might expect the anatomical network as a whole to have a shorter path length, and this is indeed what we found. The fiber density of connections where an age effect was detectable decreased in many connections, disproportionately in the frontal cortex, while it increased in some connections, disproportionately in the temporal and parietal cortices (Figure 5).

In the left hemisphere analyses, we found linear effects of increasing clustering, global efficiency and modularity with age. In the right hemisphere, we found opposite trends of linear decreases in clustering, global efficiency, small-worldness, and modularity with age. It is curious that the left hemisphere shows trends opposite to the right, and to the network as a whole; this may point to different developmental processes occurring within each hemisphere (Paus et al., 1999; Scheibel et al., 1985; Shaw et al., 2009; Sowell et al., 2003). It appears that these results are driven by asymmetries in the adults for global efficiency and modularity, as both were higher in the left hemisphere than the right for adults, but roughly the same for the 12 year olds. Trends for the clustering coefficient may also be due to anatomical asymmetries for both age groups. Recent work from our laboratory studied asymmetry of these measures in the same sample, finding greater small-worldness in the right hemisphere (Daianu et al., 2012). Our results are contrary to those of Iturria-Medina et al. (2011), who found greater global efficiency in the right hemisphere, but these were from a relatively small sample of 11 subjects, and our sample is over 40 times larger. One possible explanation is the consistent finding of right/left asymmetry in overall cerebral hemispheric volume, with the right hemisphere being larger on average (Bilder et al., 1994; Giedd et al., 1996). The asymmetry of the many structural and functional features of the brain has long been noted (Hellige, 1993; Toga & Thompson, 2003), with researchers finding asymmetry in FA (Büchel et al., 2004) and regional volumes (Good et al., 2001), as well as finding that the level of asymmetry in fiber integrity was heritable (Jahanshad et al., 2010).

For the nodal analyses, we found many linear and non-linear age effects, for all four of the nodal metrics tested. For betweenness centrality, there were more decreases with age than increases, perhaps demonstrating network refinement as fibers are pruned from some connections. Betweenness centrality shows how “central” a node is to the network, based on how many of the shortest paths go through that node. The clustering coefficient increased in about the same number of nodes as it decreased with age - this network measure refers to how many of a node’s neighbors are also connected to each other. For both betweenness centrality and the clustering coefficient, we could not discern any obvious pattern in the nodal locations of the increases or decreases. The nodal degree reflects the number of nodes a given node is connected to, and we found roughly equal representations of statistically significant increases in degree and decreases in degree with age. However, in the frontal cortex, many more nodes *decreased* in degree than increased. Conversely, of the nodes in the temporal cortex showing an age effect, more increased in degree than decreased. Similarly, we found roughly equal increases and decreases in regional efficiency with age, but there were more frontal nodes that decreased in efficiency than increased, and more temporal nodes that increased in efficiency than decreased. This may be a manifestation of the more protracted developmental trajectory of the frontal lobe compared to other lobes (Gogtay et al., 2004), or it may point to different processes occurring in different regions of the brain. A

few of these nodes also had significant age^2 terms that fit in the opposite direction, suggesting that these age effects plateaued in early adulthood. Gong et al. (2009) also reported more increases in regional efficiency in the temporal cortex with age, but they were examining a different age range (19–85). Regional efficiency is a nodal measure related to global efficiency, computed on node neighborhoods.

Tests of age effects on the 70×70 connectivity matrices revealed that fiber density decreased in more connections than it increased, but these decreases were distributed disproportionately around the brain. Follow-up analyses on the absolute fiber density data confirm that a decrease in proportional fiber density truly reflects a decrease in absolute fiber density, rather than just a more modest increase than average. Connections to and from the frontal cortex disproportionately decreased with age, relative to the changes detected in other brain regions (Figures 3 and 5, Supplementary Video 2). This was partially due to lower overall variance in the frontal cortex relative to both the temporal or parietal cortices, and also due to the greater effect sizes detected in the frontal cortex (and parietal cortex) than in the temporal cortex. Conversely, those connections leading to and from regions in the temporal cortex showed disproportionately more fiber density increases with age (Figure 3 and 5, Supplementary Video 1). Of all the significant age-related changes in fiber density, 57% were decreases and 43% were increases. Within the significant changes in connections that terminate in the frontal cortex, however, 70% were decreases and 30% were increases. Of the significant changes in the temporal cortex, 43% were decreases and 57% were increases. In the occipital cortex, 55% were decreases and 45% were increases. In the parietal cortex, 52% were decreases and 48% were increases. This mirrors the distribution of our nodal results assessing regional efficiency: the nodal degree is likely a driving factor behind these nodal results.

Prior work has revealed different developmental trajectories for the volumes of different cortical gray matter regions as well as lobar volumes that include white matter as well (Gogtay et al., 2004; Sowell et al., 2003). Giedd et al. (1999) found that the temporal cortex tended to achieve its peak for both gray and white matter volume at a later age than other lobar brain regions. Sowell et al. (2003) found that gray matter density (GMD) in the superior frontal sulcus steadily declined from age 7 on, but it increased in the superior temporal sulcus until age 30, after which it steadily declined. They found this same inverted U-shaped trajectory for a number of temporal regions, but the frontal regions all showed a steady decline in GMD from age 7 on. These findings were supported by similar results from a previous study (Sowell et al., 2002a). Several processes are active throughout development, and if they occur at different rates across the cortex, they could lead to these different trajectories and patterns of differences. Huttenlocher (1979; 1990) found different rates of synaptic pruning across the cortex. Additionally, continuing myelination (Bartzokis, 2004; Bartzokis et al., 2010), and the addition of new neurons (reviewed by Gould, 2007) may contribute to the changes we report here.

Studies of callosal development during adolescence show developmental increases in volume or cross-sectional area for the splenium and isthmus (Thompson et al., 2000; Chung et al., 2001), suggesting an increase with age in the level of myelination and/or axon count for interhemispheric connections traveling through those regions. The splenium and isthmus connect the temporal, parietal, and occipital cortices with their counterparts on the opposite hemisphere, as well as with some other cortical regions (Hofer & Frahm, 2006; Witelson, 1989). All of our 7 interhemispheric connections with detectable age effects had a terminus in the parietal lobe or posterior cingulate. This is perhaps most likely to be due to increased myelination (Bartzokis et al., 2010).

We found a few sex differences in global and nodal connectivity as well. Females had greater small-worldness and gamma (which are related measures) in whole brain parameters. Gamma (normalized clustering coefficient) is a measure of network segregation as it measures how many of a nodes neighbors are interconnected. This result suggests that females have more clustered, highly segregated networks than males do. Females also had greater degree in the left temporal pole, while males had greater degree in the right *pars orbitalis* and greater efficiency in the left precuneus and right *pars orbitalis*. While there are both consistent and conflicting results when it comes to sex differences in the brain (Kimura, 2000), a number of previous studies have noted proportionally larger temporal lobes in females than males (Harasty et al., 1997; Sowell, et al., 2002b; Luders et al., 2009) with thicker cortices (Sowell et al., 2007), possibly contributing to this effect on degree and efficiency. Gong et al. (2009), found greater global and local efficiency in females, which we did not, but they did find greater regional efficiency in females in temporal nodes and greater regional efficiency in males in frontal nodes, which overlaps with our results. Yan et al. (2011), found similar results, also revealing a sex by brain size interaction, where smaller brains showed higher local efficiency in women but not on men. Studies of sex differences in brain structural networks are important for possibly explaining the differences in susceptibility to disease or outcome after brain injury (Turkheimer & Farace, 1992). Future work should investigate whether these differences have any consequences for sex differences in cognition or vulnerability to disease, or if they are simply due to allometry (non-proportional scaling of brain structures relative to body size; Brun et al., 2010).

One limitation of the current study is the uneven sampling of the different age ranges, due to the availability of cohorts assessed at 12 and 16 but not in between. Nonparametric regression models may therefore be more appropriate for deriving *p*-values for the fitted regression coefficients. Obviously, the specific parcellation scheme chosen will affect graph theory metrics. Zalesky et al. (2010) found that graph theory metrics were sensitive to parcellation resolution (i.e., the number of nodes), but Hagmann et al. (2010) found very similar developmental trajectories at two different parcellation resolutions. Other future parcellation schemes may be more sensitive to developmental effects, but the Desikan-Killiany atlas has been shown by our laboratory to yield connectivity measures that are genetically influenced (Jahanshad et al., 2011; Jahanshad et al., 2012); it was one of the atlases used by Hagmann et al. (2010).

5. Conclusions

In summary, we found that structural brain networks decrease in path length, clustering, small-worldness, and modularity with age, although this effect may differ by hemisphere. We found significant sex differences in nodal measures of connectivity, but it remains to be seen whether these differences are related to any sex differences in cognitive function or in resilience to disease. Graph theory metrics have been associated with disease and cognitive function (Brown et al., 2011; Langer et al., 2011; Li et al., 2009), so investigating this difference further may shed light on sex differences in aspects of cognition or disease vulnerability. Defining the expected developmental trajectory of structural connectivity measures in healthy individuals is critical for gauging the effect of neuropsychiatric disorders, and ultimately of interventional factors, on development.

Supplementary Material

Refer to Web version on PubMed Central for supplementary material.

Acknowledgments

This study was supported by the National Institute of Child Health and Human Development (R01 HD050735), and the National Health and Medical Research Council (NHMRC 486682, 1009064), Australia. Genotyping was supported by NHMRC (389875). Additional support for algorithm development was provided by NIH R01 grants EB008432, EB008281, EB007813 and P41 RR013642. ED was funded, in part, by an NIH Training Grant in Neurobehavioral Genetics (T32MH073526-06). NJ was funded, in part, by an NLM Training Grant (T15 LM07356).

References

Achard S, Bullmore E. Efficiency and cost of economical brain functional networks. PLoS Comput Biol. 2007; 3:e17. [PubMed: 17274684]

Aganj I, Lenglet C, Sapiro G. Reconstruction of the orientation distribution function in single- and multiple- shell q- ball imaging within constant solid angle. Magnetic Resonance in Medicine. 2010; 64(2):554–566. [PubMed: 20535807]

Aganj I, Lenglet C, Jahanshad N, Yacoub E, Harel N, Thompson PM, Sapiro G. A Hough transform global probabilistic approach to multiple-subject diffusion MRI tractography. Medical Image Analysis. 2011; 15(4):414–425. [PubMed: 21376655]

Annett M. A classification of hand preference by association analysis. British Journal of Psychology. 1970; 61(3):303–321. [PubMed: 5457503]

Bartzokis G. Quadratic trajectories of brain myelin content: unifying construct for neuropsychiatric disorders. Neurobiology of Aging. 2004; 25:49–62.

Bartzokis G, Lu PH, Tingus K, Mendez MF, Richard A, Peters DG, Oluwadara B, Barrall KA, Finn JP, Villablanca P, Thompson PM, Mintz J. Lifespan trajectory of myelin integrity and maximum motor speed. Neurobiology of Aging. 2010; 31(9):1554–1562. [PubMed: 18926601]

Bassett DS, Bullmore E, Verchinski BA, Mattay VS, Weinberger DR, Meyer-Lindenberg A. Hierarchical organization of human cortical networks in health and schizophrenia. Journal of Neuroscience. 2008; 28(37):9239–9248. [PubMed: 18784304]

Benjamini Y, Hochberg Y. Controlling the false discovery rate: a practical and powerful approach to multiple testing. Journal of the Royal Statistical Society Series B. 1995; 57(1):289–300.

Bilder RM, Wu H, Bogerts B, Degreef G, Ashtari M, Alvir JM, Snyder PJ, Lieberman JA. Absence of regional hemisphere volume asymmetries in first episode schizophrenia. Am J Psychiatry. 1994; 151:1437–1447. [PubMed: 8092337]

Brown JA, Terashima KH, Burggren AC, Ercoli LM, Miller KJ, Small GW, Bookheimer SY. Brain network local interconnectivity loss in aging APOE-4 allele carriers. PNAS. 2011; 108(51): 20760–20765. [PubMed: 22106308]

Brun C, Lepore N, Luders E, Chou Y. Sex differences in brain structure in auditory and cingulate regions. NeuroReport. 2009; 20(10):930–935. [PubMed: 19562831]

Büchel C, Raedler T, Sommer M, Sach M, Weiller C, Koch MA. White matter asymmetry in the human brain: a Diffusion Tensor MRI study. Cerebral Cortex. 2004; 14(9):945–951. [PubMed: 15115737]

Bullmore ET, Bassett DS. Brain Graphs: Graphical Models of the Human Brain Connectome. Reviews in Advance. 2010:1–37.

Casey BJ, Giedd JN, Thomas KM. Structural and functional brain development and its relation to cognitive development. Biological Psychiatry. 2000; 54:241–257.

Chung MK, Worsley KJ, Paus T, Cherif C, Collins DL, Giedd JN, Rapoport JL, Evans AC. A unified statistical approach to deformation-based morphometry. NeuroImage. 2001; 14:595–606. [PubMed: 11506533]

Daianu, M.; Jahanshad, N.; Dennis, E.; Toga, AW.; de Zubicaray, G.; Martin, NG.; Wright, MJ.; Hickie, I.; Thompson, PM. Left versus right hemisphere differences in brain connectivity: 4-Tesla HARDI tractography in 569 twins. Proc. 9th IEEE ISBI; Barcelona. 2012. (to appear) 2012

de Zubicaray GI, Chiang M-C, McMahon KL, Shattuck DV, Toga AW, Martin NG, Wright MJ, Thompson PM. Meeting the challenges of neuroimaging genetics. Brain Imaging and Behavior. 2008; 2:258–263. [PubMed: 20016769]

Dennis EL, Jahanshad N, Rudie JD, Brown JA, Johnson K, McMahon KL, de Zubicaray GI, Montgomery G, Martin NG, Wright MJ, Bookheimer SY, Dapretto M, Toga AW, Thompson PM. Altered structural brain connectivity in healthy carriers of the autism risk gene, *CNTNAP2*. Brain Connectivity. 2012a; 1(6):447–459. [PubMed: 22500773]

Dennis, EL.; Jahanshad, N.; Toga, A.; Brown, J.; Rudie, J.; Bookheimer, S.; Dapretto, M.; Johnson, K.; McMahon, K.; de Zubicaray, G.; Martin, N.; Wright, M.; Thompson, P. Heritability of structural brain connectivity network measures in 188 twins. Proc. 41st Annual Meeting of the Society for Neuroscience; 12 to 16 November 2011; Washington, D.C..

Dennis, EL.; Jahanshad, N.; Toga, A.; Johnson, K.; McMahon, K.; de Zubicaray, G.; Martin, N.; Hickie, IB.; Wright, M.; Thompson, P. changes in anatomical brain connectivity between ages 12 and 30: A HARDI study of 467 adolescents and adults. Proc. 9th IEEE ISBI; Barcelona. 2012b. (to appear) 2012.

Dennis, EL.; Jahanshad, N.; Toga, AW.; McMahon, KL.; de Zubicaray, GI.; Martin, NG.; Wright, MJ.; Thompson, PM. Test-retest Reliability of Graph Theory Measures of Structural Brain Connectivity. Proc. 15th MICCAI; Nice. 2012c. (to appear) 2012.

Desikan R, Ségonne F, Fischl B, Quinn B. An automated labeling system for subdividing the human cerebral cortex on MRI scans into gyral based regions of interest. NeuroImage. 2006; 31:968–980. [PubMed: 16530430]

Dimond; Beaumont. Hemisphere Function in the Human Brain. Oxford, England: John Wiley & Sons; 1974.

Dosenbach NUF, Nardos B, Cohen AL, Fair DA, Power JD, Church JA, Nelson SM, Wig GS, Vogel AC, Lessov-Schlaggar CN, Barnes KA, Dubis JW, Feczko E, Coalson RS, Pruett JR, Barch DM, Petersen SE, Schlaggar BL. Prediction of Individual Brain Maturity Using fMRI. Science. 2010; 329(5997):1358–1361. [PubMed: 20829489]

Giedd JN, Blumenthal J, Jeffries NO, Castellanos FX, Liu H, Zijdenbos A, Paus T, Evans AC, Rapoport JL. Brain development during childhood and adolescence: a longitudinal MRI study. Nature Neuroscience. 1999; 2(10):861–863.

Giedd JN, Snell JW, Lange N, Rajapakse JC, Casey BJ, Kozuch PL, Vaituzis AC, Vauss YC, Hamburger SD, Kaysen D, Rapoport JL. Quantitative magnetic resonance imaging of human brain development: Ages 4–18. Cerebral Cortex. 1996; 6(4):551–559. [PubMed: 8670681]

Gogtay N, Giedd JN, Lusk L, Hayashi KM, Greenstein D, Vaituzis AC, Nugent TF III, Herman DH, Clasen LS, Toga AW, Rapoport JL, Thompson PM. Dynamic mapping of human cortical development during childhood through early adulthood. PNAS. 2004; 101(21):8174–8179. [PubMed: 15148381]

Gong G, He Y, Evans AC. Brain connectivity: Gender makes a difference. The Neuroscientist. 2011; 17(5):575–591. [PubMed: 21527724]

Gong G, Rosa-Neto P, Carbonell F, Chen ZJ, He Y, Evans AC. Age-and gender-related differences in the cortical anatomical network. Journal of Neuroscience. 2009; 29(50):15684–15693. [PubMed: 20016083]

Good CD, Johnsrude IS, Ashburner J, Henson RNA, Friston KJ, Frackowiak SJ. A voxel-based morphometric study of ageing in 465 normal adult human brains. NeuroImage. 2001; 14:21–36. [PubMed: 11525331]

Gould E. How widespread is adult neurogenesis in mammals? Nature Reviews Neuroscience. 2007; 8:481–488.

Hagmann P, Sporns O, Madan N, Cammoun L, Pienaar R, Wedeen VJ, Meuli R, Thiran J-P, Grant PE. White matter maturation reshapes structural connectivity in the late developing human brain. Proceedings of the National Academy of Sciences. 2010; 107(44):19067–19072.

Harasty J, Double K, Halliday G, Kril J. Language-associated cortical regions are proportionally larger in the female brain. Archives of Neurology. 1997; 54(2):171–176. [PubMed: 9041858]

He Y, Chen Z, Evans A. Structural insights into aberrant topological patterns of large-scale cortical networks in Alzheimer's disease. Journal of Neuroscience. 2008; 28:4756–4766. [PubMed: 18448652]

Hellige, JB. Hemispheric asymmetry: What's right and what's left. Cambridge, MA: Harvard University Press; 1993.

Hofer S, Frahm J. Topography of the human corpus callosum revisited – comprehensive fiber tractography using diffusion tensor magnetic resonance imaging. NeuroImage. 2006; 32(3):989–994. [PubMed: 16854598]

Holmes C, Hoge R, Collins L. Enhancement of MR images using registration for signal averaging. Journal of Computer Assisted Tomography. 1998; 22(2):324–333. [PubMed: 9530404]

Huttenlocher P. Synaptic density in the human frontal cortex – developmental changes and effects of aging. Brain Res. 1979; 163(2):195–205. [PubMed: 427544]

Huttenlocher P. Morphometric study of human cerebral cortex development. Neuropsychologia. 1990; 28(6):517–527. [PubMed: 2203993]

Iturria-Medina Y, Fernández AP, Morris DM, Canales-Rodríguez EJ, Haroon HA, Pentón LG, Augath M, García LG, Logothetis N, Parker GJM, Melie-García L. Brain hemispheric structural efficiency and interconnectivity rightward asymmetry in human and nonhuman primates. Cerebral Cortex. 2011; 21:56–67. [PubMed: 20382642]

Jackson, DN. Multidimensional Aptitude Battery II. Port Huron, MI: Sigma Assessment Systems; 1998.

Jahanshad, N.; Aganj, I.; Lenglet, C.; Joshi, A.; Jin, Y.; Barysheva, M.; McMahon, KL.; de Zubicaray, GI.; Martin, NG.; Wright, MJ.; Toga, AW.; Sapiro, G.; Thompson, PM. Sex differences in the human connectome: 4-tesla high angular resolution diffusion imaging (HARDI) tractography in 234 young adult twins. Proc. 8th IEEE ISBI; Chicago. 2011. p. 939-943.

Jahanshad, N.; Hibar, DP.; Ryles, A.; McMahon, KL.; de Zubicaray, GI.; Martin, NG.; Wright, MJ.; Toga, AW.; Thompson, PM. Discovery of genes that affect human brain connectivity: a genome-wide analysis of the connectome. Proc. 9th IEEE ISBI; Barcelona. 2012. (to appear) 2012.

Jahanshad N, Lee A, Barysheva M, McMahon KL, de Zubicaray GI, Martin NG, Wright MJ, Toga AW, Thompson PM. Genetic influences on brain asymmetry: A DTI study of 374 twins and siblings. NeuroImage. 2010; 52:455–469. [PubMed: 20430102]

Khundrakpam BS, Reid A, Brauer J, Carbonell F, Lewis J, Ameis S, Karama S, Lee J, Chen Z, Das S, Evans AC. Brain Development Cooperative Group. Developmental changes in organization of structural brain networks. Cerebral Cortex. 2012 in press.

Kimura, D. Sex and Cognition. Cambridge, MA: MIT Press; 2000.

Kintali S. Betweenness Centrality: Algorithms and Lower Bounds. 2008 arXiv, 0809.1906v0802.

Kochunov P, Williamson DE, Lancaster J, Fox P, Cornell J, Blangero J, Glahn DC. Fractional anisotropy of water diffusion in cerebral white matter across the lifespan. Neurobiology of Aging. 2010:1–12.

Langer N, Pedroni A, Gianotti LR, Hänggi J, Knoch D, Jäncke L. Functional brain network efficiency predicts intelligence. Human Brain Mapping. 2011 in press.

Latora V, Marchiori M. Efficient behavior of small-world networks. Physical Review Letters. 2001; 87(19):1–4.

Lenroot RK, Gogtay N, Greenstein DK, Molloy E, Wallace GL, Clasen LS, Blumenthal JD, Lerch J, Zijdenbos AP, Evans AC, Thompson PM, Giedd JN. Sexual Dimorphism of Brain Developmental Trajectories during Childhood and Adolescence. NeuroImage. 2007 published online, April 6 2007.

Leow A, Huang S, Geng A, Becker J, Davis S, Toga A, Thompson P. Inverse consistent mapping in 3D deformable image registration: its construction and statistical properties. Processing in Medical Imaging. 2005; 3565:23–57.

Li Y, Liu Y, Li J, Qin W, Li K, Yu C. Brain anatomical network and intelligence. PLoS Computational Biology. 2009; 5(5):1–17.

Luders E, Gaser C, Narr K, Toga AW. Why sex matters: brain size independent differences in gray matter distributions between men and women. The Journal of Neuroscience. 2009; 29(45):14265–14270. [PubMed: 19906974]

Paus T, Zijdenbos A, Worsley K, Collins DL, Blumenthal J, Giedd JN, Rapoport JL, Evans AC. Structural maturation of neural pathways in children and adolescents: In vivo study. Science. 1999; 283(5409):1908–1911. [PubMed: 10082463]

Rubinov M, Sporns O. Complex network measures of brain connectivity: uses and interpretations. NeuroImage. 2010; 52:1059–1069. [PubMed: 19819337]

Scheibel AB, Paul LA, Fried I, Forsythe AB, Tomiyasu U, Wechsler A, Kao A, Slotnick J. Dendritic organization of the anterior speech area. Experimental Neurology. 1985; 87(1):109–117. [PubMed: 3967694]

Shaw P, Kabani NJ, Lerch JP, Eckstrand K, Lenroot R, Gogtay N, Greenstein D, Clasen L, Evans A, Rapoport JL, Giedd JN, Wise SP. Neurodevelopmental Trajectories of the Human Cerebral Cortex. Journal of Neuroscience. 2008; 28(14):3586–3594. [PubMed: 18385317]

Shaw P, Lalonde F, Lepage C, Rabin C, Eckstrand K, Sharp W, Greenstein D, Evans A, Giedd JN, Rapoport J. Development of cortical asymmetry in typically developing children and its disruption in attention-deficit/hyperactivity disorder. Arch of General Psychiatry. 2009; 66(8):888–896.

Sowell E, Peterson B, Kan E, Woods R, Yoshii J, Bansal R, Xu D, Zhu H, Thompson PM, Toga AW. Sex differences in cortical thickness mapped in 176 healthy individuals between 7 and 87 years of age. Cerebral Cortex. 2007; 17:1550–1560. [PubMed: 16945978]

Sowell ER, Peterson BS, Thompson PM, Welcome SE, Henkenius AL, Toga AW. Mapping cortical change across the human life span. Nature Neuroscience. 2003; 6(3):309–315.

Sowell ER, Thompson PM, Rex D, Kornsand D, Tessner KD, Jernigan TL, Toga AW. Mapping sulcal pattern asymmetry and local cortical surface gray matter distribution*in vivo*: Maturation in perisylvian cortices. Cerebral Cortex. 2002a; 12:17–26. [PubMed: 11734529]

Sowell ER, Trauner DA, Gamst A, Jernigan TL. Development of cortical and subcortical brain structures in childhood and adolescence: a structural MRI study. Developmental Medicine and Child Neurology. 2002b; 44:4–16. [PubMed: 11811649]

Sporns, O. Graph theory methods for the analysis of neural connectivity patterns. In: Kötter, R., editor. Neuroscience Databases. A Practical Guide. Boston, MA: Klüwer; 2002. p. 171-186.

Sporns, O. Networks of the Brain. Cambridge, MA: The MIT Press; 2011.

Sporns O, Chialvo DR, Kaiser M, Hilgetag CC. Organization, development and function of complex brain networks. Trends in Cognitive Sciences. 2004; 8(9):418–425. [PubMed: 15350243]

Thompson PM, Giedd JN, Woods RP, MacDonald D, Evans AC, Toga AW. Growth patterns in the developing brain detected by using continuum mechanical tensor maps. Nature. 2000; 404:190–193. [PubMed: 10724172]

Thompson, PM.; Narr, KL.; Blanton, RE.; Toga, AW. Mapping structural alterations of the corpus callosum during brain development and degeneration. In: Iacoboni, M.; Zaidel, E., editors. The Corpus Callosum. Boston, MA: Klüwer; 1999.

Thompson PM, Sowell ER, Gogtay N, Giedd JN, Vidal CN, Hayashi KM, Leow A, Nicolson R, Rapoport JL, Toga AW. Structural MRI and Brain Development. International Review of Neurobiology 2005. 2005; 67PB:285–323.

Toga AW, Thompson PM. Mapping brain asymmetry. Nature Neuroscience. 2003; 4:37–48.

Turkheimer E. A Reanalysis of Gender Differences in IQ Scores Following Unilateral Brain Lesions. Psychological Assessment. 2004; 4(4):498–501.

Witelson S. Hand and sex differences in the isthmus and genu of the human corpus callosum: A Postmortem morphological study. Brain. 1989; 112:799–835. [PubMed: 2731030]

Yan C, Gong G, Wang J, Wang D, Liu D, Zhu C, Chen ZJ, Evans A, Zang Y, He Y. Sex- and Brain Size-Related Small-World Structural Cortical Networks in Young Adults: A DTI Tractography Study. Cerebral Cortex. 2011; 21(2):449–458. [PubMed: 20562318]

Zhan, L.; Chiang, MC.; Barysheva, M.; Toga, AW.; McMahon, KL.; de Zubicaray, GI.; Meredith, M.; Wright, MJ.; Thompson, PM. How Many Gradients are Sufficient in High-Angular Resolution Diffusion Imaging (HARDI)?. Workshop on Diffusion Tensor Imaging, Medical Image Computing and Computer Assisted Intervention (MICCAI); September 10 2008; New York. 2008.

Zhan, L.; Franc, D.; Patel, V.; Jahanshad, N.; Yan, Jin; Mueller, BA.; Bernstein, MA.; Borowski, BJ.; Jack, CR., Jr; Toga, AW.; Lim, KO.; Thompson, PM. How do Spatial and angular resolution affect brain connectivity maps from Diffusion MRI?. Proc. 9th IEEE ISBI; Barcelona. 2012a. (to appear) 2012.

Zhan L, Jahanshad N, Ennis DB, Bernstein MA, Borowski BJ, Jack CR Jr, Toga AW, Leow AD, Thompson PM. Angular versus spatial resolution trade-offs for diffusion imaging under time constraints. Human Brain Mapping. 2012b Apr 25.2012

Zhan, L.; Leow, AD.; Barysheva, M.; Feng, A.; Toga, AW.; Sapiro, G.; Harel, N.; Lim, KO.; Lenglet, C.; McMahon, KL.; de Zubicaray, GI.; Wright, MJ.; Thompson, PM. Investigating the uncertainty in multi-fiber estimation in High Angular Resolution Diffusion Imaging. In: Kilian, Pohl; Sarang, Joshi; Sandy, Wells, editors. Workshop on Probabilistic Modeling in Medical Image Analysis (PMMIA), Medical Image Computing and Computer Assisted Intervention (MICCAI); September 20 2009; London. 2009b.

Zhan L, Leow AD, Chiang MC, Barysheva M, Lee AD, Toga AW, McMahon KL, de Zubicaray GI, Wright MJ, Thompson PM. How does Angular Resolution Affect Diffusion Imaging Measures? NeuroImage. 2009a Oct 9. 2009 [Epub ahead of print].

Zhan, L.; Leow, AD.; Zhu, S.; Chiang, MC.; Barysheva, M.; Toga, AW.; McMahon, KL.; de Zubicaray, GI.; Wright, MJ.; Thompson, PM. Analyzing. Multi-Fiber Reconstruction in High Angular Resolution Diffusion Imaging using the Tensor Distribution Function; Proc. 6th IEEE ISBI; Boston. 2009c. p. 1402-1405.(2009).

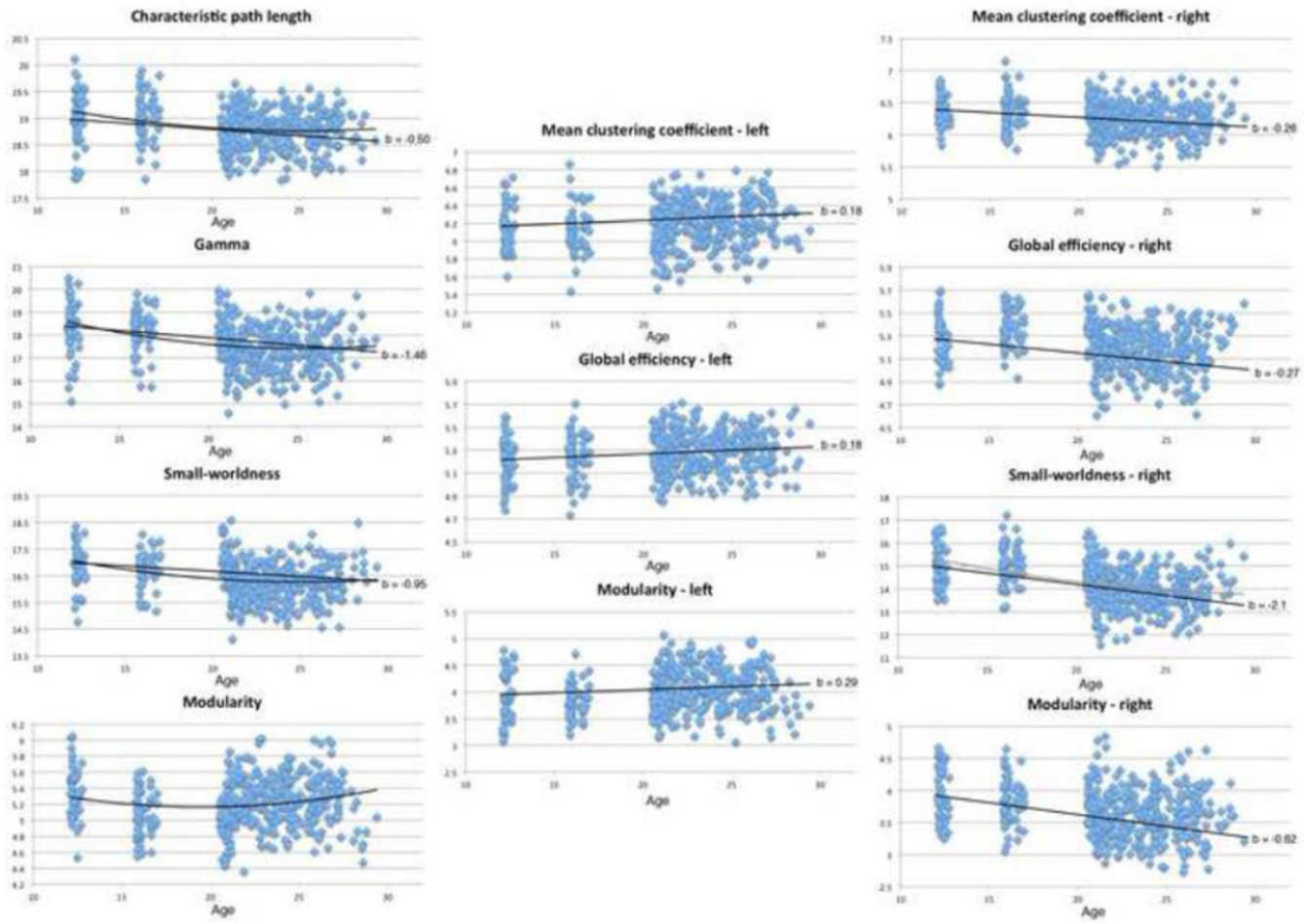

Figure 1. Scatterplots showing significant associations between global graph theory connectivity scores and *age* in whole brain, left, and right hemispheres

Linear trendlines added with slopes and *b* values (regression coefficients) corresponding to results from Tables 1–3. Slopes taken from *b* values from Eq. 2 results, no linear trendline in included for modularity (whole brain), as that analysis was not significant.

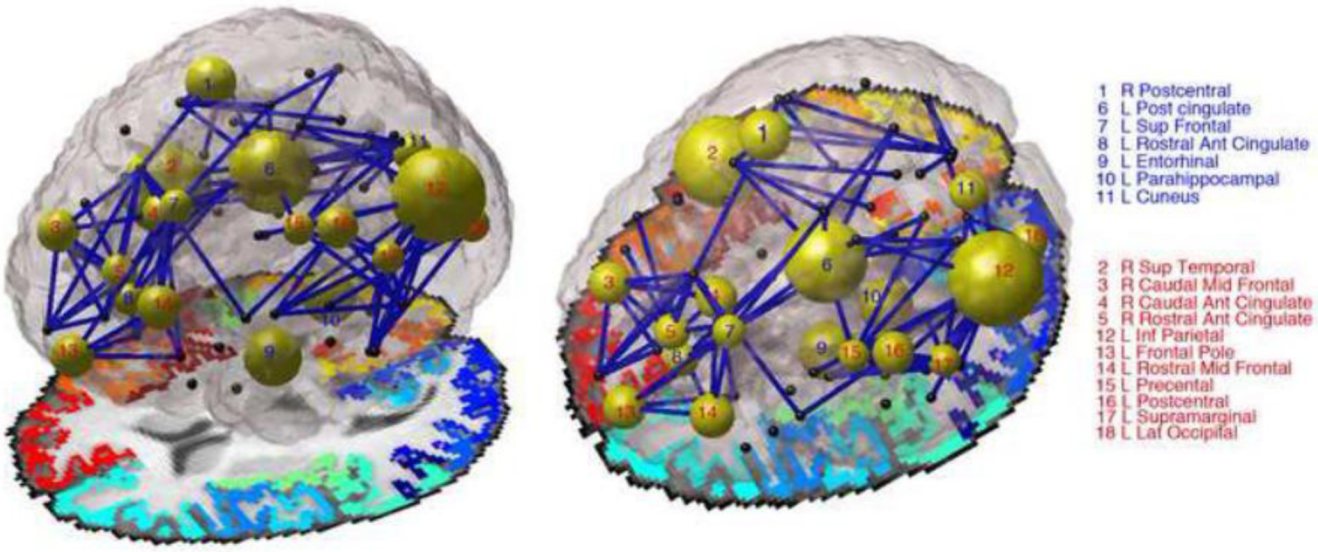

Figure 2. Image depicting developmental effects, comparing children (12 and 16 year olds) to adults (20–30 year olds)

The diameter of each node is inversely proportional to the *p*-value for the degree analyses – large diameter means node was significantly different in degree between children and adults. Non-significant nodes are colored black. Nodes numbered in blue increase in degree with age, while those numbered with red decrease in degree with age. Blue connections are those that changed with age, corresponding to significant boxes in Figure 3. For this image we looked only at connections present in at least 95% of subjects. Author NJ is the creator of this image.

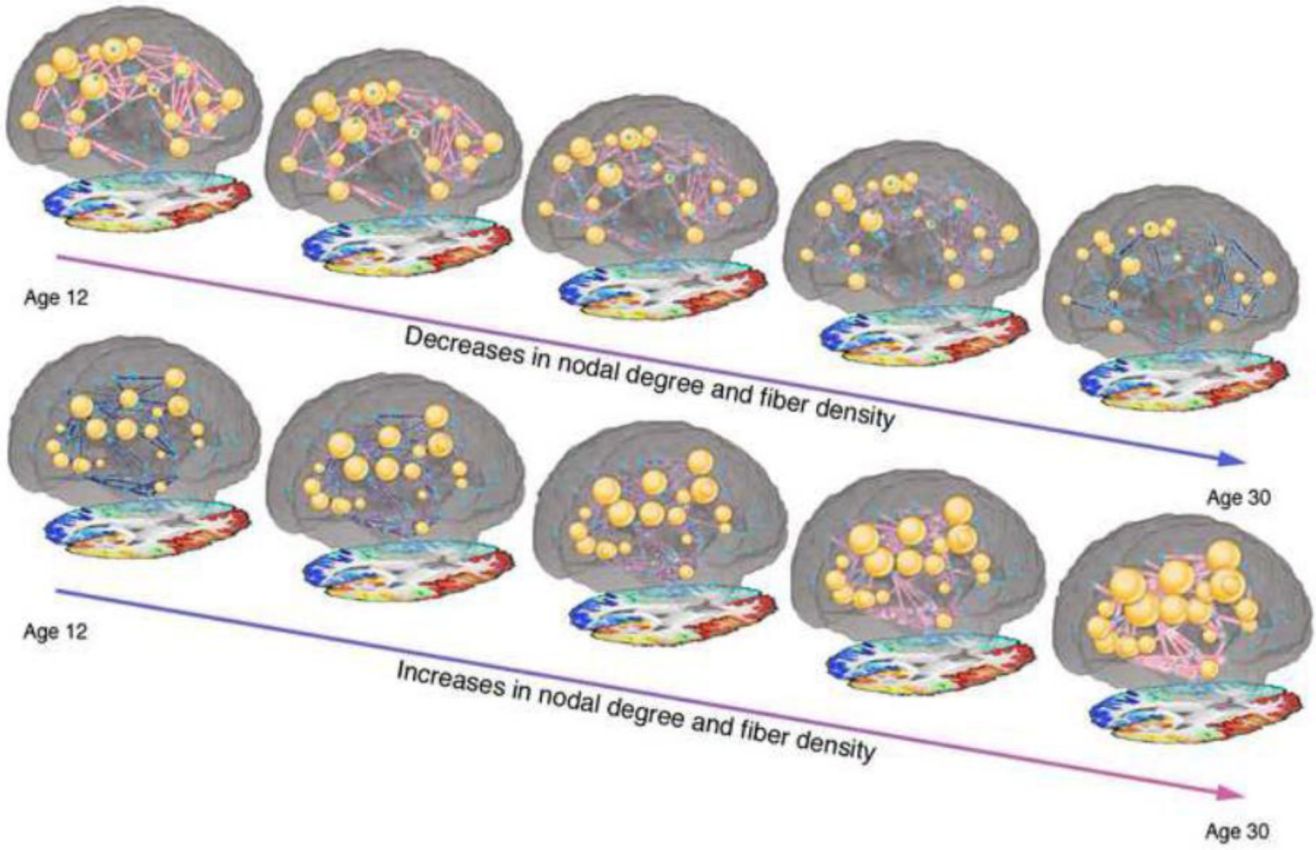

Figure 3.
Still images from Supplementary Video 1 and Supplementary Video 2 displaying the increases and decreases in degree and fiber density between age 12 and age 30. While we lack scan data for some parts of this age range, we used the regression coefficients from our analysis to estimate network metrics at each year.

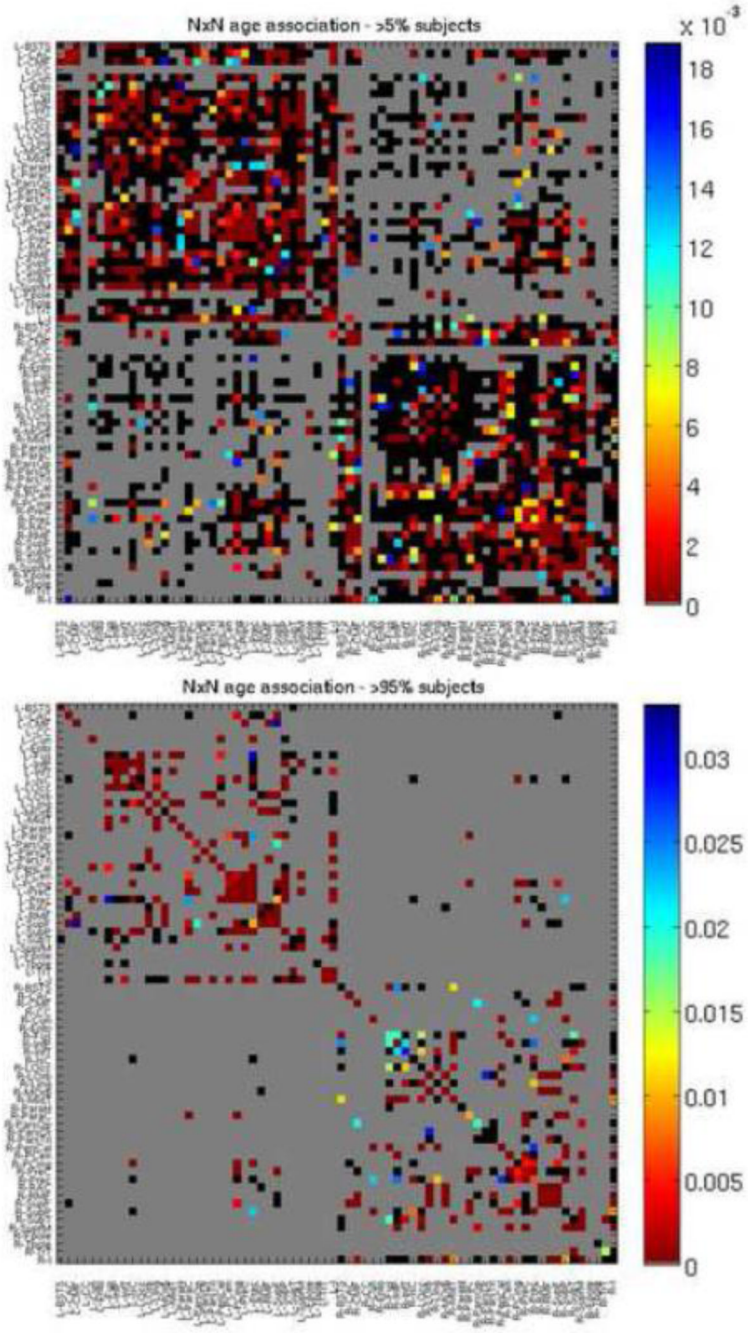

Figure 4. *P* map of *age* effects, when modeled alone (Eq. 2), with 70×70 fiber density matrix from which graph theory metrics were calculated

Colors correspond to strength of p value as indicated by color bar. Gray boxes were not tested as those connections were not present. For the top p map connections that were present in at least 5% of subjects were tested, for the bottom p map, connections that were present in at least 95% of subjects were tested. Black boxes were tested but not significant. FDR corrected ($q < 0.05$). See Table 6 for region key.

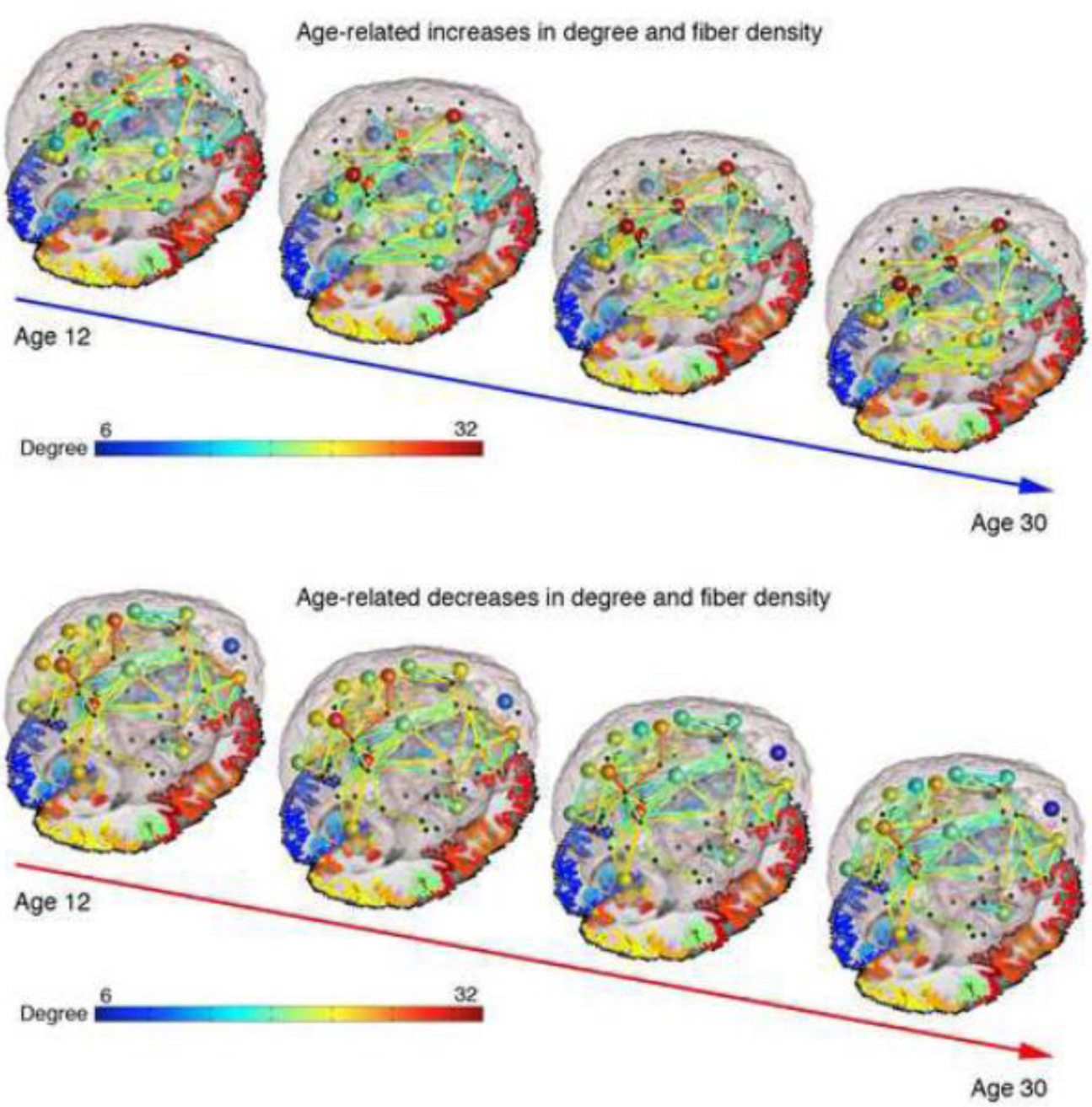

Figure 5. Image depicting developmental trajectory, with averaged networks shown for four groups (12 year olds, 16 year olds, 20–24 year olds, 24–30 year olds)

The color of each connection is proportional to the average fiber density within group with red signifying the thickest connections and blue the thinnest connections; the color of the node is proportional to the average degree of that node within group. For this image we looked only at connections present in at least 95% of subjects. Author NJ is the creator of this image.

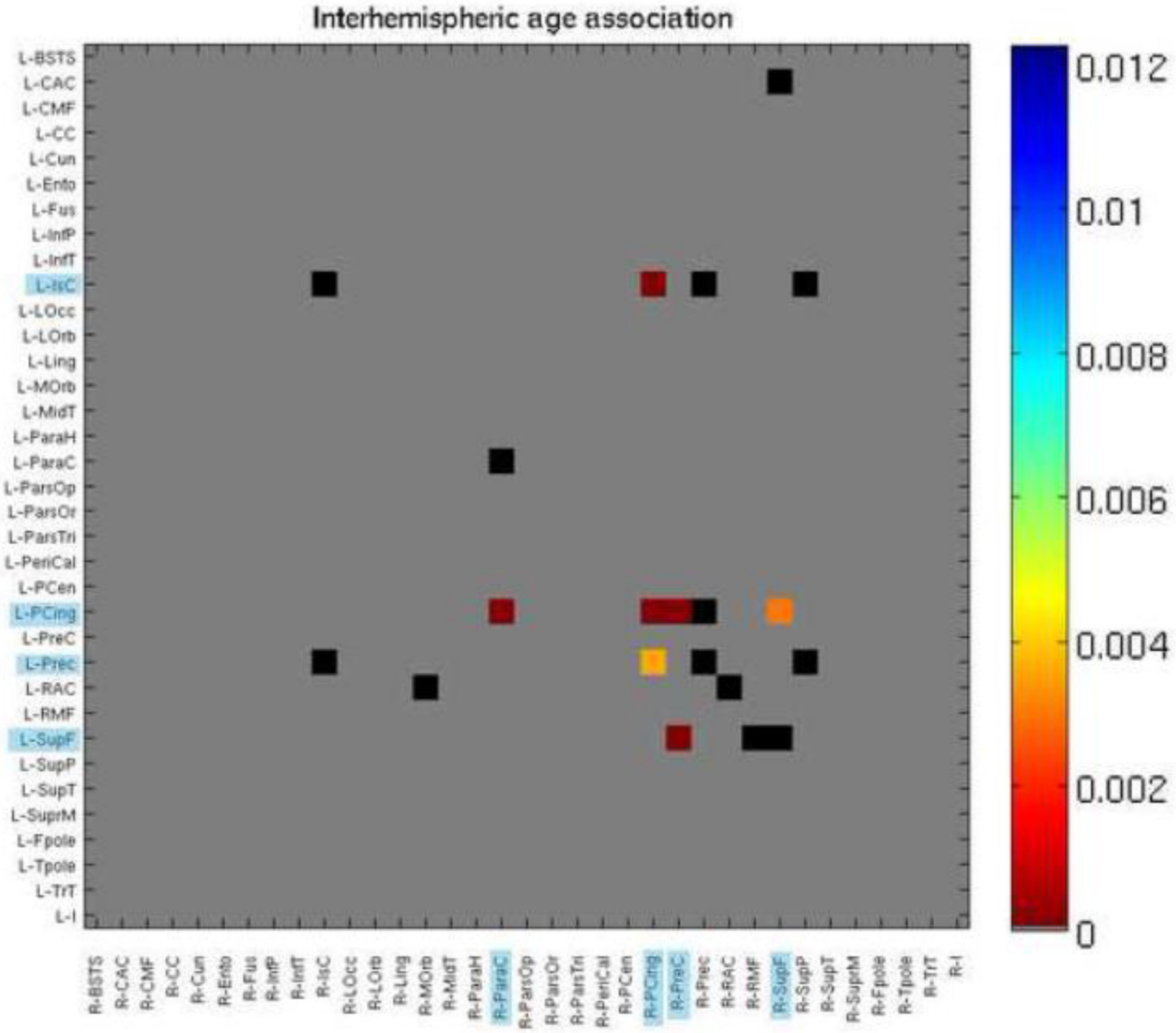

Figure 6. *P* maps of *age* effects, when modeled alone (Eq. 2), with 35×35 interhemispheric fiber density matrix

Colors correspond to strength of *p* value as indicated by color bar. Blue highlighting on regions indicate significance. Gray boxes were not tested as those connections were not present. Black boxes were tested but not significant. FDR corrected ($q < 0.05$). See Table 6 for region key.

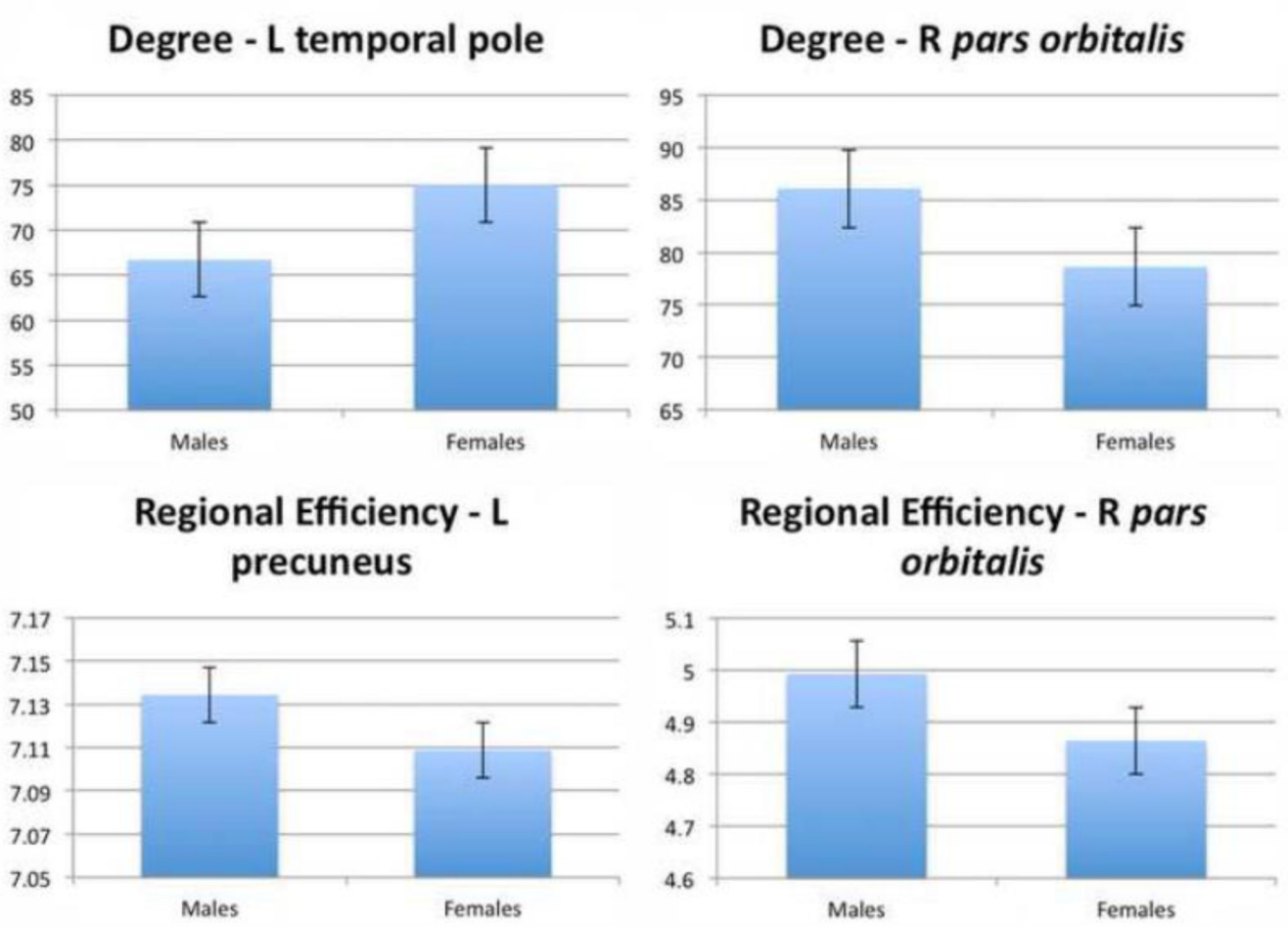

Figure 7. Bar graphs of nodes showing significant sex effects for degree (integrated over range of sparsities)

FDR corrected ($q < 0.05$).

Table 1

Demographics of study sample

IQ was not collected for the 12-year-old cohort. yo = year old.

Group	N	Mean Age (SD)	M/F	FIQ	PIQ	VIQ
Adults	337	23.6 (2.19)	126/211	112	115	115
Kids	102	14.4 (1.95)	49/53	112	119	117
12 yo	55	12.3 (0.18)	24/31	NA	NA	NA
16 yo	47	16.2 (0.37)	25/22	112	119	117

Table 2

Effects of *age* and *age*^{2}, both modeled together (Eq. 1) and just *age* (Eq. 2) on global connectivity metrics for the whole brain

FDR corrected within model, with left and right hemisphere analyses FDR corrected separately from whole brain analyses.

***Age* and *Age*^{2} combined (Eq. 1)**		
	Age	***Age*^{2}**
Characteristic path length/Lambda	**−0.11 (0.0043) / −0.038 (0.0073)**	**0.050 (0.022)** / 0.024 (0.033)
Mean clustering coefficient/Gamma	ns / **−0.38 (0.00018)**	ns / **0.18 (0.0018)**
Global efficiency	ns	ns
Small-worldness	**−0.26 (0.00053)**	**0.13 (0.0034)**
Modularity	**−0.077 (0.013)**	**0.044 (0.013)**
	Sex	
Small-worldness	**0.018 (0.011)**	
Gamma	**0.022 (0.020)**	
***Age* (Eq. 2)**		
	Age	
Characteristic path length/Lambda	**$-0.023\ (1.0\times10^{-6})$ / $-0.011\ (1.9\times10^{-6})$**	
Mean clustering coefficient/Gamma	ns / **$-0.066\ (8.0\times10^{-8})$**	
Global efficiency	ns	
Small-worldness	**$-0.043\ (3.1\times10^{-6})$**	
Modularity	ns	
	Sex	
Small-worldness	0.014 (0.034)	

Table 3

Effects of *age* and *age*^{2}, both modeled together (Eq. 1) and just *age* (Eq. 2) on global connectivity metrics for the left hemisphere

FDR corrected as described for Table 1 ($q < 0.05$).

***Age* and *Age*^{2} combined (Eq. 1)**		
	Age	***Age*^{2}**
Characteristic path length/Lambda	ns / ns	ns / ns
Mean clustering coefficient/Gamma	ns / ns	ns / ns
Global efficiency	ns	ns
Small-worldness	ns	ns
Modularity	ns	ns
***Age* (Eq. 2)**		
	Age	
Characteristic path length/Lambda	ns / −0.0054 (0.021)	
Mean clustering coefficient/Gamma	**0.0082 (0.0036)** / −0.024 (0.027)	
Global efficiency	**0.0082 (3.6×10^{-5})**	
Small-worldness	ns	
Modularity	**0.013 (0.0043)**	

Table 4

Effects of *age* and *age2*, both modeled together (Eq. 1) and just *age* (Eq. 2) on global connectivity metrics for the right hemisphere

FDR corrected as described for Table 1 ($q < 0.05$).

***Age* and *Age2* combined (Eq. 1)**		
	Age	***Age*^{2}**
Characteristic path length/Lambda	ns / ns	ns / ns
Mean clustering coefficient/Gamma	−0.054 (0.033) / −0.28 (0.0041)	ns / ns
Global efficiency	ns	ns
Small-worldness	−0.27 (0.0022)	0.10 (0.041)
Modularity	−0.086 (0.025)	ns
	Sex	
Global efficiency	0.0050 (0.0079)	
***Age* (Eq. 2)**		
	Age	
Characteristic path length/Lambda	ns / ns	
Mean clustering coefficient/Gamma	**$-0.012\ (5.7\times10^{-5})$ / $-0.095\ (4.2\times10^{-15})$**	
Global efficiency	**$-0.012\ (1.9\times10^{-7})$**	
Small-worldness	**$-0.095\ (3.7\times10^{-16})$**	
Modularity	**$-0.028\ (1.4\times10^{-9})$**	
	Sex	
Global efficiency	**0.0050 (0.01)**	

Table 5

Effects of *age* and *age*^{2} together on nodal graph theory metrics, as modeled by Eq. 1

'ns' corresponds to non-significant effect. FDR corrected within model across all nodal metrics tested ($q < 0.05$). Bolded entries survive FDR across all metrics and all nodes within model. Non-bolded entries were survived FDR within metric but did not survive FDR across all metrics tested.

	Betweenness Centrality	Clustering	Degree	Regional Efficiency
Age				
L Cuneus	ns	ns	**10 (0.0035)**	ns
L Entorhinal	ns	ns	**13 (0.00024)**	ns
L Inferior Parietal	**−72 (4.6×10^{-6})**	**0.24 (0.00052)**	**−12 (1.2×10^{-4})**	**−0.10 (4.5×10^{-4})**
L Lat Occipital	**−54 (3.7×10^{-5})**	**0.25 (0.0021)**	−7.2 (0.0059)	ns
L Parahippocampal	ns	**−0.50 (9.6×10^{-3})**	**14 (0.00043)**	**0.16 (0.00020)**
L Paracentral	**−130 (0.0011)**	ns	ns	ns
L Postcentral	−24 (0.0069)	ns	**−9.1 (0.0025)**	−0.072 (0.0088)
L Post Cingulate	**220 (0.00044)**	**−0.22 (3.4×10^{-6})**	**19 (6.4×10^{-4})**	**0.14 (6.9×10^{-4})**
L Precentral	**−120 (0.00088)**	ns	−9.5 (0.0099)	−0.082 (0.0051)
L Rostral Ant Cingulate	ns	ns	10 (0.0096)	ns
L Rostral Mid Frontal	**−95 (0.0012)**	**0.26 (0.0020)**	**−10 (0.0017)**	**−0.091 (0.0040)**
L Sup Frontal	ns	ns	11 (0.0085)	0.086 (0.0055)
L Supra-marginal	ns	ns	−5.9 (0.010)	ns
L Frontal Pole	ns	ns	**−8.2 (0.0020)**	−0.34 (0.0053)
R Caudal Ant Cingulate	−44 (0.0086)	**0.21 (0.0029)**	**−11 (0.0026)**	−0.091 (0.0075)
R Isthmus of the Cingulate	−100 (0.011)	ns	ns	ns
R Parahippocampal	ns	ns	ns	0.12 (0.0056)
R Paracentral	−54 (0.0049)	ns	ns	ns
R Postcentral	ns	**−0.34 (5.1×10^{-6})**	**12 (0.00065)**	**0.10 (0.0014)**
R Precuneus	**−190 (0.0026)**	ns	ns	ns
R Rostral Ant Cingulate	−63 (0.0052)	ns	−7.7 (0.0054)	ns
R Rostral Mid Frontal	ns	ns	**−7.2 (0.0021)**	ns
R Sup Temporal	**−50 (0.0012)**	ns	**−9.5 (2.1×10^{-4})**	**−0.091 (2.9×10^{-5})**
R Supra-marginal	ns	ns	ns	0.077 (0 0066)
Age^2				
L Entorhinal	ns	ns	**−6.3 (0.0010)**	ns
L Inferior Parietal	**32 (0.00033)**	ns	**5.0 (0.00020)**	**0.050 (0.00023)**
L Parahippocampal	ns	**0.22 (0.0021)**	ns	ns
L Post Cingulate	ns	**0.95 (0.00047)**	**−8.2 (0.00088)**	**−0.054 (0.0011)**
R Postcentral	ns	**0.17 (6.9×10^{-5})**	ns	ns
R Sup Temporal	ns	ns	**5.0 (2.5×10^{-5})**	**0.045 (0.00019)**

Table 6

Effects of *age* alone on nodal graph theory metrics, as modeled by Eq. 2 and Eq. 3

All 70 connections were tested but only those significant in one of the analyses are included in the table in the interest of space. 'ns' corresponds to non-significant effect. FDR corrected ($q < 0.05$). All entries included survive FDR within model across all four metrics tested and all nodes tested.

	Betweenness Centrality	Clustering	Degree	Regional Efficiency
Age				
L Caudal Ant Cingulate	ns	−0.032 (7.4×10^{-05})	2.7 (0.0054)	0.022 (0.0031)
L Caudal Mid Frontal	ns	−0.022 (0.024)	−1.4 (0.025)	ns
L Cuneus	ns	−0.037 (0.0029)	2.6 (7.5×10^{-09})	0.027 (8.7×10^{-09})
L Entorhinal	ns	0.10 (0.0039)	1.5 (0.00025)	0.050 (0.00012)
L Fusiform	16 (0.0022)	−0.037 (0.00036)	1.6 (6.8×10^{-05})	0.019 (1.8×10^{-07})
L Inferior Parietal	−17 (2.0×10^{-16})	0.059 (9.3×10^{-13})	−2.9 (3.0×10^{-20})	−0.023 (1.5×10^{-14})
L Isthmus of the Cingulate	35 (0.00033)	−0.028 (9.7×10^{-07})	3.6 (3.0×10^{-12})	0.027 (2.6×10^{-12})
L Lat Occipital	−14 (5.4×10^{-17})	0.072 (3.1×10^{-12})	−2.2 (1.6×10^{-11})	−0.020 (6.5×10^{-09})
L Lat Orbitofrontal	ns	0.042 (0.00050)	−1.6 (0.011)	ns
L Lingual	ns	−0.031 (0.00080)	1.6 (5.0×10^{-06})	0.014 (6.5×10^{-06})
L Mid Temporal	−4.4 (0.00023)	0.031 (0.0020)	−1.4 (0.00016)	−0.013 (0.0013)
L Parahippocampal	8.2 (0.0038)	−0.11 (2.4×10^{-12})	4.2 (5.7×10^{-17})	0.044 (2.5×10^{-16})
L Paracentral	−27 (3.2×10^{-08})	ns	ns	ns
L Pars opercularis	ns	ns	−0.95 (0.0017)	ns
L Pars orbitalis	−0.50 (0.021)	ns	−0.82 (0.00041)	−0.0086 (0.025)
L Pars triangularis	ns	ns	−0.91 (0.0065)	ns
L Peri-calcarine	11 (0.0030)	−0.045 (3.1×10^{-06})	2.1 (3.8×10^{-06})	0.018 (5.34×10^{-06})
L Postcentral	−7.7 (7.8×10^{-12})	0.063 (4.3×10^{-11})	−3.1 (1.3×10^{-14})	−0.025 (8.0×10^{-13})
L Post Cingulate	59 (3.1×10^{-14})	−0.059 (1.7×10^{-20})	5.4 (6.5×10^{-21})	0.040 (6.2×10^{-22})
L Precentral	−23 (3.6×10^{-07})	0.023 (0.011)	−2.0 (7.2×10^{-06})	−0.014 (4.9×10^{-05})
L Precuneus	−23 (0.0056)	ns	1.1 (0.0020)	0.0086 (0.0017)
L Rostral Ant Cingulate	54 (2.8×10^{-14})	−0.063 (3.8×10^{-14})	3.3 (1.6×10^{-11})	0.028 (1.2×10^{-10})
L Rostral Mid Frontal	−26 (2.7×10^{-12})	0.063 (4.0×10^{-10})	−4.0 (2.2×10^{-19})	−0.034 (1.6×10^{-17})
L Sup Frontal	42 (8.2×10^{-06})	−0.028 (7.1×10^{-07})	3.0 (4.7×10^{-09})	0.024 (5.3×10^{-10})
L Sup Parietal	−28 (1.2×10^{-13})	0.034 (1.7×10^{-07})	−1.9 (2.9×10^{-08})	−0.016 (3.4×10^{-08})
L Supra-marginal	−7.7 (9.8×10^{-06})	ns	−1.5 (7.8×10^{-08})	−0.0082 (0.00057)
L Frontal Pole	ns	ns	−2.5 (9.9×10^{-14})	−0.054 (0.00014)
L Transverse Temporal	ns	−0.072 (6.9×10^{-12})	1.6 (2.4×10^{-06})	0.020 (3.7×10^{-05})
L Insula	ns	−0.015 (0.0018)	0.68 (0.015)	0.0082 (0.00093)
R Caudal Ant Cingulate	−12 (2.2×10^{-08})	0.033 (9.8×10^{-05})	−2.1 (6.3×10^{-07})	−0.014 (0.00025)
R Caudal Mid Frontal	−6.8 (0.00081)	ns	ns	ns
R Entorhinal	ns	0.14 (6.5×10^{-05})	ns	ns

	Betweenness Centrality	Clustering	Degree	Regional Efficiency
R Isthmus of the Cingulate	−15 (0.0012)	ns	ns	ns
R Lat Occipital	−20 (1.4×10^{-09})	0.039 (9.8×10^{-05})	−1.1 (0.00020)	−0.010 (0.00095)
R Lingual	15 (0.011)	−0.034 (0.00014)	1.0 (0.0060)	0.011 (0.0026)
R Med Orbitofrontal	ns	ns	−1.8 (0.0020)	−0.014 (0.0085)
R Mid Temporal	11 (3.1×10^{-09})	−0.054 (1.4×10^{-07})	1.8 (1.0×10^{-08})	0.018 (4.7×10^{-08})
R Paracentral	−7.7 (0.00048)	0.038 (0.00014)	−1.3 (0.0025)	−0.0086 (0.021)
R Pars opercularis	3.9 (4.5×10^{-08})	−0.042 (1.2×10^{-05})	1.6 (3.2×10^{-06})	0.020 (2.5×10^{-07})
R Postcentral	8.2 (4.9×10^{-05})	−0.045 (1.6×10^{-07})	2.6 (2.2×10^{-09})	0.022 (6.3×10^{-08})
R Post Cingulate	−12 (0.00065)	0.015 (0.022)	ns	ns
R Precentral	−18 (0.00024)	ns	ns	ns
R Precuneus	−38 (1.1×10^{-06})	0.022 (3.9×10^{-05})	−1.1 (0.0017)	−0.0077 (0.0070)
R Rostral Ant Cingulate	−6.3 (0.014)	ns	−1.4 (9.2×10^{-06})	−0.010 (0.0014)
R Rostral Mid Frontal	−20 (2.2×10^{-06})	0.032 (5.2×10^{-06})	−1.8 (3.8×10^{-11})	−0.013 (4.4×10^{-07})
R Sup Temporal	−6.3 (0.0010)	0.026 (0.0090)	−1.2 (6.2×10^{-07})	−0.011 (1.9×10^{-05})
R Supra-marginal	15 (1.2×10^{-10})	−0.041 (2.0×10^{-09})	2.3 (5.5×10^{-09})	0.027 (5.6×10^{-14})
R Transverse Temporal	ns	ns	1.1 (0.00060)	0.012 (0.0021)

Table 7

Distribution of significant age-related effects on 4 nodal measures tested, with increases and decreases separated.

	Betweenness centrality		Clustering coefficient		Degree		Regional efficiency		Number of nodes belonging to each lobe
	Incr.	Decr.	Incr.	Decr.	Incr.	Decr.	Incr.	Decr.	
Frontal	4	10	6	6	5	13	5	9	26
Temporal	3	2	4	5	7	2	7	2	20
Parietal	3	8	5	3	4	5	4	5	14
Occipital	2	2	2	4	4	2	4	2	8

Table 8

List of 10 most significant age-related increases and 10 most significant age-related decreases in proportional fiber density when *age* is examined alone. When only one region is listed, an age-related increase or decrease in the proportion of fibers going through that node was found.

Top 10 increases in fiber density	
Connection	***b-val***
L Supramarginal × L Inferior Parietal	−0.000358
R Caudal Middle Frontal	−0.000347
L Lateral Orbitofrontal × L Rostral Mid Frontal	−0.000255
L Med Orbitofrontal × L Rostral Mid Frontal	−0.000314
L Postcentral × L Insula	−0.000276
L Insula × L Supramarginal	−0.000429
L Inferior Parietal	−0.00108
L Supramarginal × L Posterior Cingulate	−0.000296
L Sup Frontal × L Rostral Mid Frontal	−0.000483
R Sup Frontal × R Rostral Ant Cingulate	−0.000309
Top 10 decreases in fiber density	
Connection	*b-val*
L Posterior Cingulate	0.00337
L Paracentral × L Posterior Cingulate	0.00143
L Posterior Cingulate × L Precuneus	0.000967
L Posterior Cingulate × L Sup Frontal	0.000999
R Postcentral × R Insula	0.000593
L Isthmus of the Cingulate	0.00277
R Postcentral	0.000956
L Sup Frontal × R Prefrontal	0.000168
L Isthmus of the Cingulate × L Precuneus	0.00176
L Caudal Ant Cingulate × L Sup Frontal	0.00101

Table 9

Region key

Abbreviation	Region	Abbreviation	Region
L-BSTS	L Banks of the Superior Temporal Sulcus	R-BSTS	R Banks of the Superior Temporal Sulcus
L-CAC	L Caudal Anterior Cingulate	R-CAC	R Caudal Anterior Cingulate
L-CMF	L Caudal Middle Frontal	R-CMF	R Caudal Middle Frontal
L-CC	L Corpus Callosum	R-CC	R Corpus Callosum
L-Cun	L Cuncus	R-Cun	R Cuncus
L-Ento	L Entorhinal	R-Ento	R Entorhinal
L-Fus	L Fusiform	R-Fus	R Fusiform
L-InfP	L Inferior Parietal	R-InfP	R Inferior Parietal
L-InfT	L Inferior Temporal	R-InfT	R Inferior Temporal
L-IsC	L Isthmus of the Cingulate	R-IsC	R Isthmus of the Cingulate
L-LOcc	L Lateral Occipital	R-LOcc	R Lateral Occipital
L-LOrb	L Lateral Orbitofrontal	R-LOrb	R Lateral Orbitofrontal
L-Ling	L Lingual	R-Ling	R Lingual
L-MOrb	L Medical Orbitofrontal	R-MOrb	R Medical Orbitofrontal
L-MidT	L Middle Temporal	R-MidT	R Middle Temporal
L-ParaH	L Parahippocampal	R-ParaH	R Parahippocampal
L-ParaC	L Paracentral	R-ParaC	R Paracentral
L-ParsOp	L Pars opercularis	R-ParsOp	R Pars opercularis
L-ParsOr	L Pars orbitalis	R-ParsOr	R Pars orbitalis
L-ParsTri	L Pars triangularis	R-ParsTri	R Pars triangularis
L-PeriCal	L Peri-calcarine	R-PeriCal	R Peri-calcarine
L-PCen	L Postcentral	R-PCen	R Postcentral
L-PCing	L Posterior Cingulate	R-PCing	R Posterior Cingulate
L-PreC	L Precentral	R-PreC	R Precentral
L-Prec	L Precuneus	R-Prec	R Precuneus
L-RAC	L Rostral Anterior Cingulate	R-RAC	R Rostral Anterior Cingulate
L-RMF	L Rostral Middle Frontal	R-RMF	R Rostral Middle Frontal
L-SupF	L Superior Frontal	R-SupF	R Superior Frontal
L-SupP	L Superior Parietal	R-SupP	R Superior Parietal
L-SupT	L Superior Temporal	R-SupT	R Superior Temporal
L-SuprM	L Supra-marginal	R-SuprM	R Supra-marginal
L-Fpole	L Frontal Pole	R-Fpole	R Frontal Pole
L-Tpole	L Temporal Pole	R-Tpole	R Temporal Pole
L-TrT	L Transverse Temporal	R-TrT	R Transverse Temporal
L-I	L Insula	R-I	R Insula

Table 10

Sex differences in nodal measures of connectivity

Males were coded as '1' and females as '2', thus a positive b value indicates greater nodal scores in females. FDR corrected ($q < 0.05$).

	Degree	Regional Efficiency
L Precuneus	ns	−0.0082 (0.00057)
L Temporal Pole	1.3 (0.00038)	ns
R *Pars orbitalis*	−0.91 (0.00049)	$-0.019\ (8.5\times10^{-5})$